# Three-Dimensional Electromagnetic Power Deposition in Tumors Using Interstitial Antenna Arrays

CYNTHIA M. FURSE AND MAGDY F. ISKANDER, SENIOR MEMBER, IEEE

*Abstract*—**Interstitial arrays of insulated antennas have shown promise for microwave hyperthermia treatment of deep-seated tumors. Available analytical techniques for predicting the electromagnetic (EM) power deposition of these antennas have been limited to the case of a homogeneous conductive medium surrounding the array. Since tumors and host tissue may differ in their electrical characteristics, it is necessary to consider the impact of this variation in electrical properties and the geometry of the tumor in the calculation of the EM field distribution and power deposition pattern when modeling interstitial antennas.**

**In this paper a three-dimensional model of a tumor of arbitrary shape subjected to the fields of an interstitial antenna array is developed to predict the EM power deposition in an inhomogeneous tumor-tissue medium. The volume integral equation for the imbedded tumor is developed and solved by method of moments. The incident fields are calculated based on the available formulation of interstitial antennas in homogeneous media. The accuracy of the developed computer code was checked by comparing the results from the volume integral approach with the Mie solution for the special case of spherical tumors. Good comparison was obtained for tumors with properties approximately 25 percent different from those of the surrounding tissue. Comparisons of results from models of antenna arrays with and without imbedded tumors show significant differences in their predictions of the EM power deposition in the tumor.**

**Hyperthermia protocols generally specify uniform temperature distribution within the tumor. The developed inhomogeneous model was used to examine the feasibility of controlling the uniformity of the power deposition pattern in large tumors by adjusting the amplitude or relative phase between the array elements. Results are presented to show that a phase lead of +90° or relative amplitude of 4.0 on one antenna in a square array of four antennas could be used to shift the power deposition pattern to sequentially heat outer portions of a 2 cm diameter tumor, thereby achieving a more uniform time-averaged temperature distribution in the tumor.**

## I. INTRODUCTION

INTERSTITIAL arrays of insulated antennas have shown promise for microwave hyperthermia treatment of deep-seated tumors. This method of invasive hyperthermia has recently generated increased interest because of its compatibility with invasive radiation therapy and other surgical procedures. Invasive hyperthermia is particularly well-suited for heating deep-seated tumors, as it overcomes the problems of low penetration depth and surface burns associated with many other (noninvasive) methods [1]–[5].

Therapeutic application of invasive hyperthermia requires an understanding of the expected temperature distribution in the tumor and surrounding tissues. This can be accomplished by calculating the electromagnetic power deposition pattern and then using it in the Bioheat equation to predict temperature distribution [6]. Available analytical techniques for predicting the electromagnetic (EM) power deposition of interstitial antenna arrays have been limited to the case of antennas imbedded in homogeneous media [7]. Since tumors and host tissue may differ in their electrical properties [8]–[12], it is necessary to consider the impact of this variation in electrical properties and the geometry of the tumor on the EM field distribution and their resulting power deposition.

In this paper a three-dimensional model of a tumor of arbitrary shape subjected to the fields of an interstitial antenna array is developed to predict the EM power deposition in an inhomogeneous tumor-issue medium. The incident fields on the tumor are calculated using the model developed by Trembly for an interstitial array of insulated antennas immersed in a homogeneous medium [7]. The volume integral equation for the scattering from the tumor is then developed and solved by method of moments. The accuracy of the solution was checked by comparing the results obtained using the volume integral approach with those calculated from the Mie solution for the special case of spherical tumors. Good comparisons were obtained, and results for a variety of tumor geometries were then calculated. Comparison of the results from models of antenna arrays with and without imbedded tumors show significant differences in their predictions of the EM power deposition.

Furthermore, since hyperthermia protocols generally specify uniform temperature distribution within the tumor, we used the developed inhomogeneous model to investigate changing the relative phase between various elements of the antenna array to shift the power deposition pattern and sequentially heat outer portions of large tumors, thereby achieving a more uniform time-averaged tumor temperature distribution.

The developed numerical model will be described in Section II, its accuracy will be validated in Section III, and results from a variety of tumor models will be dis-

Manuscript received May 2, 1988; revised November 21, 1988.

The authors are with the Department of Electrical Engineering, University of Utah, Salt Lake City, UT 84112.

IEEE Log Number 8929833.

0018-9294/89/1000-0977$01.00 © 1989 IEEE

cussed in Section IV. Data showing the effectiveness of changing the phase between the array elements to control the power deposition pattern will be presented in Section V.

## II. Development of Numerical Model

It is desired to develop a three-dimensional model of a tumor of arbitrary shape, with relative permittivity $\epsilon_r(r)$ and conductivity $\sigma(r)$, imbedded in a host tissue with electrical properties $\epsilon_{r_{ext}}$ and $\sigma_{ext}$, and surrounded by an interstitial antenna array as shown in Fig. 1. The effect of scattering by the tumor can be obtained by replacing the tumor with an equivalent current source $\bar{J}eq$ where

$$\bar{J}eq(\bar{r}) = \tau(\bar{r})\bar{E}(\bar{r}) = \left[\left(\sigma(\bar{r}) - \sigma_{ext}\right) + j\omega\epsilon_0\left(\epsilon_r(\bar{r}) - \epsilon_{r_{ext}}\right)\right]\bar{E}(\bar{r}). \quad (1)$$

The first term in (1) is the conduction current term, while the second term is displacement current, and $\bar{E}(\bar{r})$ is the electric field within the tumor.

The scattered field from the tumor may be expressed in terms of $\bar{J}eq$ using the tensor Green's function $\boldsymbol{G}(\bar{r}, \bar{r}')$. Since it will be necessary to evaluate this field inside the tumor where singularity and uniqueness problems exist, the form given by Van Bladel [14] is used. The scattered field is then expressed

$$\bar{E}^s(\bar{r}) = PV\int_v \bar{J}eq(\bar{r}) \cdot \boldsymbol{G}(\bar{r}, \bar{r}')\, dv' - \frac{\bar{J}eq(\bar{r})}{3j\omega\epsilon^*_{ext}} \quad (2)$$

where

$$\boldsymbol{G}(\bar{r}, \bar{r}) = -j\omega\mu_0\left[1 + \frac{\nabla\nabla}{k^2_{ext}}\right]\Psi(\bar{r}, \bar{r}') \quad (3)$$

$$\Psi(\bar{r}, \bar{r}') = \frac{\exp\left(-jk_{ext}|\bar{r} - \bar{r}'|\right)}{4\pi|\bar{r} - \bar{r}'|} \quad (4)$$

$$\epsilon^*_{ext} = \epsilon_0\epsilon_{r_{ext}} + \frac{j\sigma_{ext}}{\omega\epsilon_0}$$

$$k_{ext} = \omega\left(\mu_0\epsilon^*_{ext}\right)^{1/2}.$$

$\mu_0$ is the permeability of free space, and $PV$ denotes the principle value of the integral as defined by Van Bladel [14].

The total electric field within the tumor can then be written as the sum of the incident electric field $\bar{E}^i$ and the scattered electric field $\bar{E}^s$. Thus,

$$\bar{E}(\bar{r}) = \bar{E}^i(\bar{r}) + \bar{E}^s(\bar{r}). \quad (5)$$

Substituting (1) and (2) into (5) and rearranging terms gives the volume integral equation for the inhomogeneous model [13]

$$\left[1 + \frac{\tau(\bar{r})}{3j\omega\epsilon^*_{ext}}\right]\bar{E}(\bar{r}) - PV\int_v \tau(\bar{r}')\bar{E}(\bar{r}) \cdot \boldsymbol{G}(\bar{r}, \bar{r}')\, dv' = \bar{E}^i(\bar{r}). \quad (6)$$

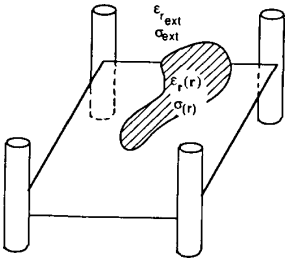


Fig. 1. Tumor of arbitrary shape with electrical properties $\epsilon_r(r)$ and $\sigma(r)$ imbedded in host tissue ($\epsilon_{r_{ext}}$, $\sigma_{ext}$) and heated by an interstitial antenna array.

This integral equation can be transformed to a matrix equation using the method of moments [13]. The tumor is subdivided into $N$ cubical cells which are chosen sufficiently small that $\tau(\bar{r})$ and $\bar{E}(\bar{r})$ may be assumed to be constant in each cell. Equation (6) may then be written as

$$\sum_{q=1}^{3}\sum_{n=1}^{N} \boldsymbol{G}^{mn}_{x_p x_q} E_{x_q}(r_n) = -E^i_{x_p}(r_m), \quad \begin{matrix} m = 1, 2, 3, \cdots, \\ p = 1, 2, 3 \end{matrix} \quad (7)$$

where $q$ and $p$ are indexes for the rectangular coordinate system with $p, q = 1$ corresponding to $x$ direction, 2 to $y$ direction, and 3 to $z$ direction.

$G^{mn}_{x_p x_q}$ is evaluated for nonself-cells ($m \neq n$) as

$$G^{mn}_{x_p x_q} = -\frac{j\omega\mu_0 k_{ext}\tau(r_n)\Delta V_n \exp\left(-j\alpha_{mn}\right)}{4\pi\alpha^2_{mn}} \cdot \left[\left(\alpha^2_{mn} - 1 - j\alpha_{mn}\right)\delta_{pq} + \cos\theta^{mn}_{x_p} \cdot \cos\theta^{mn}_{x_q}\left(3 - \alpha^2_{mn} + 3j\alpha_{mn}\right)\right], \quad m \neq n \quad (8)$$

where

$$\alpha_{mn} = k_{ext}R_{mn},\ R_{mn} = |\bar{r}_m - \bar{r}_n|$$

$$\Delta V_n = \text{volume of } n\text{th cell}$$

$$\cos\theta^{mn}_{x_p} = \frac{(x^m_p - x^n_p)}{R_{mn}} \quad \cos\theta^{mn}_{x_q} = \frac{(x^m_q - x^m_p)}{R_{mn}}$$

and $\bar{r}_m$ and $\bar{r}_n$ are the vectors

$$\bar{r}_m = (x^m_1, x^m_2, x^m_3)$$

$$\bar{r}_n = (x^n_1, x^n_2, x^n_3).$$

For the self-cell ($m = n$) $G^{mn}_{x_p x_q}$ is evaluated using Van Bladel's principle value method [14] as

$$G^{mn}_{x_p x_q} = \delta_{pq}\left\{\frac{-2j\omega\mu_0\tau(r_n)}{3k^2_{ext}} \cdot \left[\exp\left(-jk_{ext}a_n\right)\left(1 + jk_{ext}a_n\right) - 1\right] - \left[1 + \frac{\tau(r_n)}{3j\omega\epsilon^*_{ext}}\right]\right\} \quad (9)$$

where $a_n = (3\Delta V_n/4\pi)^{1/3}$.

The incident field $\bar{E}^i$ is the field produced by the antenna array and has been developed by Trembly for an array immersed in an homogeneous conducting dielectric [7]. Neglecting the coupling between the antennas, he obtains fields at any point by vector summation of the fields from each individual array element. The fields from a single insulated antenna were originally developed by King *et al.* [15].

Each insulated antenna of half-length $h$ is assumed to be made up of a center conductor (assumed perfectly conducting) of radius $a$ and a surrounding dielectric insulation of radius $b$ and relative permittivity $\epsilon_{r2}$. The fields from a single insulated antenna immersed in a conducting dielectric with relative permittivity $\epsilon_{r_{ext}}$ and conductivity $\sigma_{ext}$ are given in Appendix A.

For our model it is assumed that the antennas have sufficiently thick insulation to make them well-enough insulated from their surroundings that the scattered field from the tumor does not affect the current distribution on the antenna, and hence the incident field may be assumed unaltered by the tumor and independent of the scattering process. It is also assumed that array elements are spaced sufficiently far apart that coupling between them may be neglected. The validity of these assumptions will be examined in detail in Section III of this paper.

Upon solving (6) using the method of moments, the total electric field in each mathematical cell within the tumor is calculated. The EM power deposition is then related to the fields at any point by the specific absorption ratio (SAR) $= 0.5\sigma|E|^2$ where $\sigma$ is the conductivity at the point of interest.

## III. Verification of Results

The accuracy of the developed three-dimensional block model was checked by comparing it with the analytical Mie solution for spherical scatterers [16]. A 2 cm diameter sphere of complex permittivity $\epsilon_r = 1.362$, $\sigma = 0.002936$ S/m placed in air ($\epsilon_r = 1.0$, $\sigma = 0.0$), and illuminated by a 1 V/m plane wave at 915 MHz was numerically modeled by cubical cells. The properties of the sphere were chosen to represent the relative difference between normal brain ($\epsilon_r = 42.047$, $\sigma = 0.877$), and muscle tissue ($\epsilon_r = 55.0$, $\sigma = 1.45$) representing the tumor. The first model used was a 512-cell $2.0 \times 2.0 \times 2.0$ cm$^3$ cube. Use of symmetry allowed calculations of fields to be made in only one octant of the system, requiring 64 cells for computation. Results for $|\bar{E}|$ along the axis of the sphere parallel to the incident wave are shown in Table I. The volume integral approach and Mie solution show good agreement, differing by less than one percent near the center of the sphere and by less than seven percent at the outer edges of the sphere.

In the second numerical model, excess cells at the corners of the cube used in the previous calculations were removed to more accurately model the sphere. A total of 360 cells was then used, with the use of symmetry requiring calculation in only 45 of those cells. The results

TABLE I
Comparison of MIE and VIE Solutions for Calculated $|E|$ (V/m) Along the Axis Parallel to a 1 V/m, 915 MHz Planewave Incident on a 2 cm Diameter Conducting Dielectric Sphere ($\epsilon_r = 1.362$, $\sigma = 0.002936$) in Air ($\epsilon_r = 1.0$, $\sigma = 0.0$).

| x(cm) | (MIE) \|E\| | (VIE) \|E\| | | Percent Deviation | |
|---|---|---|---|---|---|
| | | N=512 | N=360 | N=512 | N=360 |
| -1.0 | .6961 | .8359 | .8660 | 6.7 | 3.4 |
| -.075 | .8963 | .8607 | .8888 | 4.2 | 0.9 |
| -0.50 | .8964 | .8818 | .8930 | 1.6 | 0.4 |
| -0.25 | .8964 | .8947 | .8901 | 0.2 | 0.7 |
| +0.25 | .8957 | .8947 | .8901 | 0.1 | 0.6 |
| +0.50 | .8952 | .8818 | .8930 | 1.5 | 0.2 |
| +0.75 | .8945 | .8607 | .8888 | 3.8 | 0.7 |
| +1.0 | .8936 | .8359 | .8660 | 6.4 | 3.1 |

for this case are also shown in Table I. Superb agreement between the analytical and numerical methods was observed, with less than three percent deviation at the outer edges.

Unlike previously published data [17], the agreement between the Mie solution and the volume integral equation is expected because of the relatively small difference between electrical parameters of the tumor and its host tissue. Even in [17] serious errors were observed only for corner cells of scatterers of radically different electrical properties than their surroundings. Central cells showed good agreement for all cases.

The incident fields from the interstitial array of insulated antennas shown in Fig. 2 were calculated using Trembly's homogeneous model [7]. This 3 cm square array of four antennas (each with $a = 0.333$ mm, $b = 1.0$ mm, $h = \lambda_L/4 = 3.47$ cm, $f = 915$ MHz, $\epsilon_{r2} = 2.0$) is imbedded in normal brain tissue which has $\epsilon_{r_{ext}} = 42.047$ and $\sigma_{ext} = 0.877$ S/m at 915 MHz [7]. The resulting values for $|\bar{E}|^2$ are shown in Fig. 3 as a function of vertical distance ($z$) from its central plane. Values for $z = 0$ agree with those originally reported by Trembly [7].

The stability of the method of moments numerical model may be checked by evaluating the sensitivity of the obtained results to subdividing in mathematical cells [17]. The model used for this verification is shown in Fig. 4. The $1.2 \times 1.2 \times 1.2$ cm$^3$ cubical tumor ($\epsilon_r = 55.0$, $\sigma = 1.45$ S/m, $\lambda_{tumor} = 4.3$ cm) is imbedded in normal brain tissue ($\epsilon_{r_{ext}} = 42.047$, $\sigma_{ext} = 0.877$ S/m at 915 MHz) and heated by the array shown in Fig. 2. The tumor is originally made up of 27 cubical cells, each with side $< 0.1 * \lambda_{tumor} = 0.4$ cm. Fig. 5(a) shows the normalized SAR distribution in the 27-cell model of the tumor.

The center cell is then subdivided into eight cubical subcells, each with side = 0.2 cm, so that the original volume of the tumor remains unchanged. The normalized SAR distribution for this case is shown in Fig. 5(b). There is less than one percent variation between the calculated SAR values in the subdivided cells and the corresponding undivided cell in the original model. Also less than one

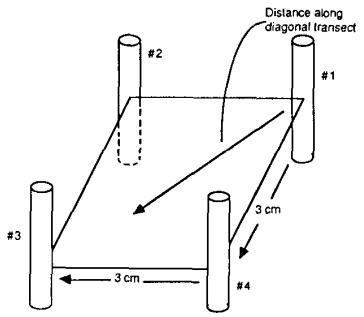


Fig. 2. 3 cm square array of four insulated antennas each with $a = 0.333$ mm, $b = 1.0$ mm, $\epsilon_{r2} = 2.0$, $h = \lambda_L/4 = 3.47$ cm, $f = 915$ MHz imbedded in a material with $\epsilon_{r_{ext}} = 42.047$, $\sigma_{ext} = 0.877$ S/m.

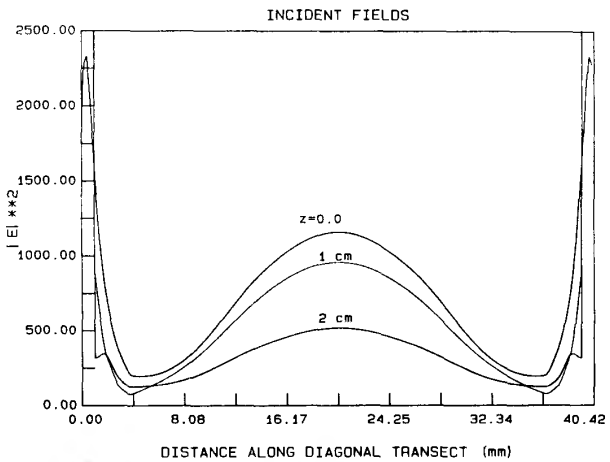


Fig. 3. $|\bar{E}|^2 (V^2/m^2)$ for interstitial antenna array shown in Fig. 2. $V_{01} = V_{02} = V_{03}$ $V_{04} = 1.0$–0.

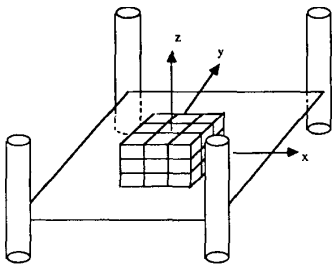


Fig. 4. A cubical tumor ($1.2 \times 1.2 \times 1.2$ cm$^3$) irradiated by the 3 cm square array of four antennas, shown in Fig. 2. $\epsilon_{r_{ext}} = 42.047$, $\sigma_{ext} = 0.877$ S/m, $\epsilon_{r_{tumor}} = 55.0$, $\sigma_{tumor} = 1.45$ S/m.

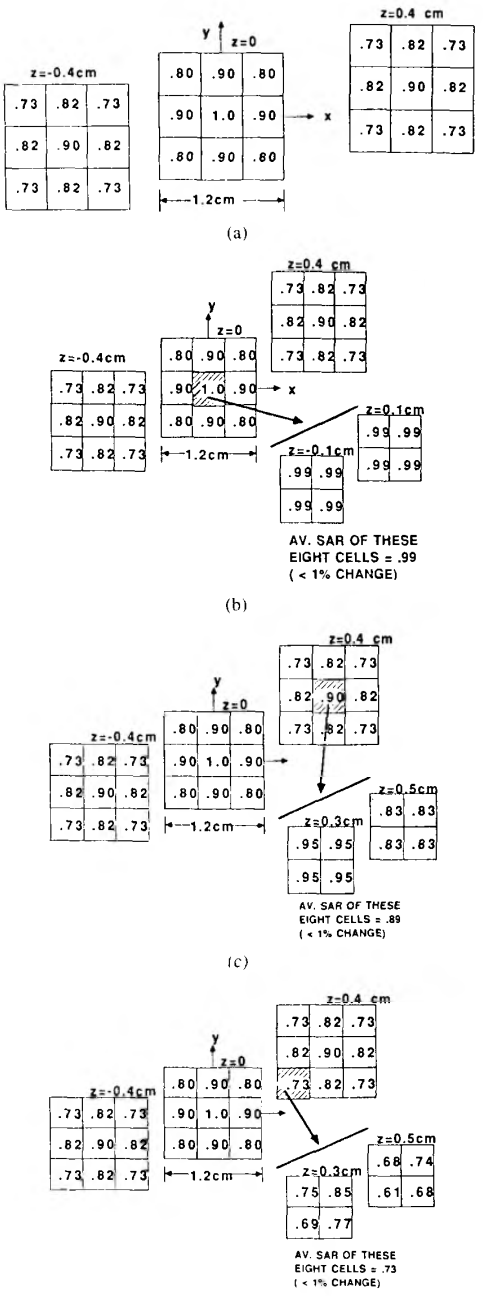


Fig. 5. Normalized SAR (W/kg) distribution in a cubical tumor block model ($1.2 \times 1.2 \times 1.2$ cm$^3$) irradiated by the 3 cm square array of four antennas shown in Fig. 2. $\epsilon_{r_{ext}} = 42.047$, $\sigma_{ext} = 0.877$ S/m, $\epsilon_{r_{tumor}} = 55.0$, $\sigma_{tumor} = 1.45$ S/m. (a) Original cubical tumor model. (b) Tumor model with subdivided center cell. (c) Tumor model with subdivided edge cell. (d) Tumor model with subdivided corner cell.

percent change is observed in calculated SAR values in neighboring cells.

Next an external cell was subdivided, again into eight subcells with sides = 0.2 cm. The calculated normalized SAR distribution is shown in Fig. 5(c). The largest variation observed between SAR values in any subcell and the original undivided cell is eight percent. The averaged SAR for these eight subcells in within two percent of that calculated in the original undivided cell, and the SAR values in neighboring cells are altered by less than one percent.

Finally, a corner cell was subdivided. The calculated normalized SAR distribution is shown in Fig. 5(d). SAR values in individual subcells differ from the original undivided cell by as much as 16 percent, but the average

SAR for all eight subcells is within one percent of that calculated for the original undivided cell. SAR values in neighboring cells are altered by less than one percent.

These observations at a glance seem to contradict earlier observations regarding the ability of the block model to predict SAR distribution [17]. This, however, is not the case simply because even in [17] the subdivisions of the mathematical cells provided accurate results unless these cells were at interfaces or corners between media of *very large discontinuity in electrical properties*. It is expected and consistently shown that for convergent solutions subdivisions of mathematical cells provide slight alterations in the results such as those reported here. We can conclude that the results from the block model are accurate for our case because the electrical characteristics of the modeled tumor and its host tissue differ by approximately 25 percent which is not a radical change in properties.

## IV. Results

Two basic assumptions were made when determining the incident fields from an array of insulated antennas. The first was that the antennas are "sufficiently insulated" from their environment that their radiated fields (incident on the tumor) are unaffected by the scattered field from the tumor. An examination of the effect of varying external medium and the thickness of the antenna insulation on the input impedance of the antenna determines what insulation thickness is necessary to support this assumption. As shown in Fig. 6, a ratio of insulation to conductor thicknesses ratio ($b/a$) of 3.0 ensures less than five percent change in input impedance even for significant changes in the external medium. Fig. 6 shows an insulation to center conductor ratio of 1.5 would be sufficient for the validity of this assumption. Since the input impedance of the antenna is the most sensitive measure of its susceptibility to the environmental changes, it follows that the current distribution will remain unchanged, and hence the radiation pattern will not be altered significantly if the input impedance remains nearly constant. It is also assumed that a tumor, which is a finite change in external medium, will affect the antenna properties even less than immersing the antenna in a completely different medium.

The second assumption regarding the incident fields is that the antennas are "sufficiently" far apart that coupling between them may be neglected. This assumption is valid if the antennas are sufficiently spaced that the field incident from one another is small. Fig. 7 shows the normalized incident field from an insulated antenna with parameters $h = 3.47$ cm, $a = 0.333$ mm, $b = 1.0$ mm, $\epsilon_{r_2} = 2.0$, $f = 915$ MHz, $\epsilon_{r_4} = 42.0$, $\sigma_4 = 0.88$ S/m. At a distance $d = 3$ cm from the antenna, the field has attenuated to ten percent of its maximum value. Thus, 3 cm should be "sufficient spacing" so that coupling between two antennas in a 3 cm array may be neglected.

To compare the fields predicted in the tumor using Trembly's homogeneous model [7] and the developed

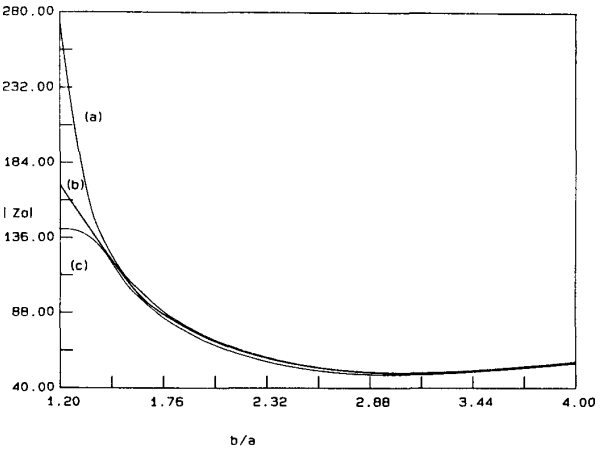


Fig. 6. Effect of changing the ratio of antenna insulation to conductor thickness ($b/a$) and external medium on $|Z_0|$ of insulated antennas. $a = 0.333$ mm, $b = 1.0$ mm, $h = \lambda_L/4 = 3.47$ cm, $f = 915$ MHz, $\epsilon_{r2} = 2.0$. (a)$\epsilon_{r_{ext}} = 30.0$ $\sigma_{ext} = 0.0$; (b) $\epsilon_{r_{ext}} = 42.047$, $\sigma_{ext} = 0.877$ S/m; (c) $= \epsilon_{r_{tumor}} = 55.0$, $\sigma_{tumor} = 1.45$ S/m.

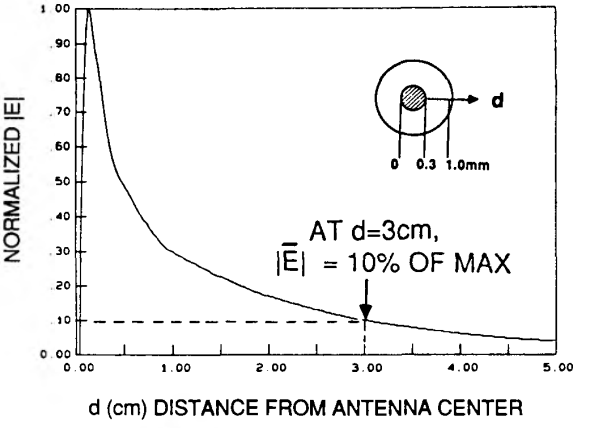


Fig. 7. Normalized $|\bar{E}|$ as a function of distance from a single insulated antenna ($h = 3.47$ cm, $a = 0.333$, $b = 1.0$ mm.

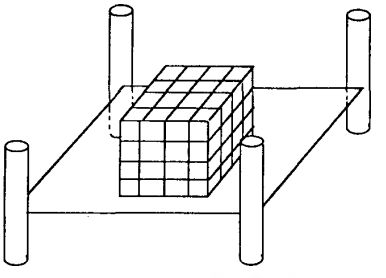

Fig. 8. A cubical tumor ($1.0 \times 1.0 \times 1.0$ cm$^3$) irradiated by a 3 cm square array of four antennas. ($a = 0.333$ mm, $b = 1.0$ mm, $h = \lambda_L/4 = 3.47$ cm, $f = 915$ MHz, $\epsilon_{r2} = 2.0$), $\epsilon_{r_{ext}} = 42.047$, $\sigma_{ext} = 0.877$ S/m, $\epsilon_{r_{tumor}} = 55.0$, $\sigma_{tumor} = 1.45$ S/m.

three-dimensional inhomogeneous model, the system shown in Fig. 8 was used. The $1.0 \times 1.0 \times 1.0$ cm$^3$ cubical tumor is heated by the square antenna array shown in Fig. 2. The physical symmetry of the system allows us to reduce the size of the matrix equation by calculating

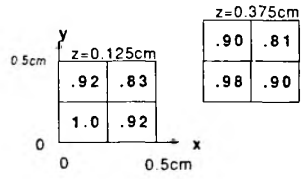


(a) $\epsilon_{r_{tumor}}/\epsilon_{r_{ext}} = 1.0$, $\sigma_{tumor}/\sigma_{ext} = 1.0$
(Homogeneous model)
Average Normalized SAR = 0.91

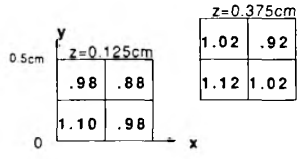


(b) $\epsilon_{r_{tumor}}/\epsilon_{r_{ext}} = 0.75$, $\sigma_{tumor}/\sigma_{ext} = 1.0$
Average Normalized SAR = 1.00
Average cell-by-cell change from (a) = 11%

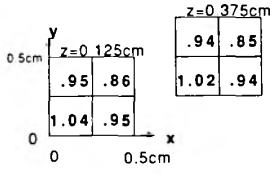


(c) $\epsilon_{r_{tumor}}/\epsilon_{r_{ext}} = 1.0$, $\sigma_{tumor}/\sigma_{ext} = 0.75$
Average Normalized SAR = 0.94

Fig. 9. $|\bar{E}|^2(V^2/m^2)$ distribution in one octant of a cubical tumor ($1 \times 1 \times 1$ cm$^3$) irradiated by a 3 cm square array of four antennas. ($a$ = 0.333 mm, $b$ = 1.0 mm, $h = \lambda_L/4$ = 3.47 cm, $f$ = 915 MHz, $\epsilon_{r2}$ = 2.0, $\epsilon_{r_{ext}}$ = 42.047, $\sigma_{ext}$ = 0.877 S/m.)

the fields in only one of the eight tumor quadrants. Fields in the remaining cells are obtained by symmetry.

The calculated distributions of normalized SAR for three different tumors with $\epsilon_{ra} = 42.047$, $\sigma_a = 0.877$ S/m; $\epsilon_{rb} = 31.54$, $\sigma_b = 0.877$ S/m; and $\epsilon_{rc} = 42.047$, $\sigma_c = 0.6575$ S/m properties are shown in Fig. 9(a)–(c). These tumors are not meant to represent specific biological tissues, but rather have electrical properties which are either the same as those of the external medium [Fig. 9(a)] or 25 percent different, in real part [Fig. (b)], or in $\sigma$ [Fig. (c)] from those of the external medium ($\epsilon_{r_{ext}} = 42.047$, $\sigma_{ext} = 0.877$ S/m).

SAR predicted in the tumor using the homogeneous model (no tumor present) is numerically equivalent to having a tumor with the same electrical properties as the external medium so for case (a) normalized SAR distributions predicted by the homogeneous and inhomogeneous model were identical. As the electrical properties of the tumor and its host tissue diverged, the SAR distributions predicted by the two models became different.

The following trends were observed:

1) Decreasing the permittivity of the tumor relative to the host tissue ($\epsilon_{r_{ext}} = 42.047$, $\sigma_{ext} = 0.877$ S/m) increased normalized SAR, as seen comparing Fig. 9(a) with (b). A 25 percent decrease in permittivity produced an 11 percent increase in SAR-averaged over the tumor.

2) Decreasing the conductivity of the tumor relative to the host tissue produces an increase in SAR as seen by

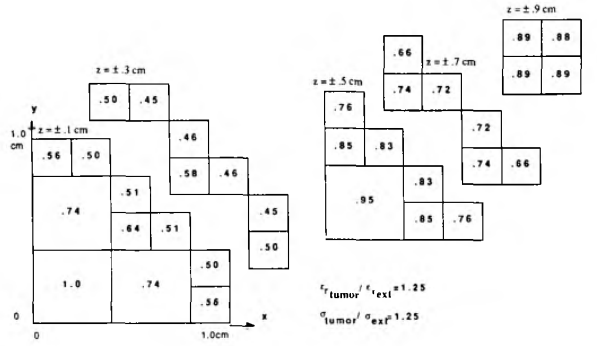


Fig. 10. Normalized SAR distribution in one octant of a 2 cm diameter tumor irradiated by a 3 cm square array of four antennas. ($a$ = 0.333 mm, $b$ = 1.0 mm, $h$ = 3.47 cm, $f$ = 915 MHz, $\epsilon_{r2} = 2.0$, $\epsilon_{r_{ext}} = 42.047$, $\sigma_{ext} = 0.877$ S/m, $\epsilon_{r_{tumor}} = 55.0$, $\sigma_{tumor} = 1.45$ S/m.)

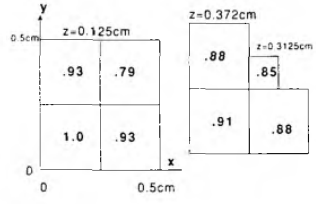


Fig. 11. Normalized SAR distribution in one octant of a 1 cm diameter tumor irradiated by a 3 cm square array of four antennas. ($a$ = 0.333 mm, $b$ = 1.0 mm, $h = \lambda_L/4$ = 3.47 cm, $f$ = 915 MHz, $\epsilon_{r2} = 2.0$, $\epsilon_{r_{ext}} = 42.047$, $\sigma_{ext} = 0.877$ S/m, $\epsilon_{r_{tumor}} = 55.0$, $\sigma_{tumor} = 1.45$ S/m.)

comparing Fig. 9(a) and (c). Since the power absorbed is proportional to conductivity (SAR = $0.5\sigma|\bar{E}|^2$ this increase offset the expected decrease in power absorption. A 25 percent decrease in conductivity produced an averaged four percent increase in normalized SAR and therefore a 21 percent decrease in actual power absorption.

Hyperthermia protocols generally specify uniform temperature distribution within the tumor. To examine numerically the possibility of producing uniform power deposition patterns in large tumors we utilized the inhomogeneous model with a 2 cm diameter (approximately) spherical tumor with cross sections shown in Fig. 10. Symmetry is applied to allow reduction of the size of the resulting matrix equation by calculating fields in only one of eight quadrants. The obtained normalized SAR distribution is shown in Fig. 10 for a tumor with electrical properties $\epsilon_r = 55.0$ and $\sigma = 1.45$ S/m and imbedded in normal brain tissue ($\epsilon_{r_{ext}} = 42.047$, $\sigma_{ext} = 0.877$ S/m) at 915 MHz. It is heated using the antenna array shown in Fig. 2 ($a$ = 0.333 mm, $b$ = 1.0 mm, $h = \lambda_L/4$ = 3.47 cm, $f$ = 915 MHz, with the dielectric constant of the insulation, $\epsilon_{r2} = 2.0$). The power absorption in the center of the tumor is calculated to be as much as 55 percent greater than in its periphery, which represents a highly nonuniform heating pattern within the tumor.

The excess power deposition in the tumor core observed in a 2 cm-diameter tumor can be compared to that of a 1 cm-diameter tumor with cross sections shown in Fig. 11. This tumor has electrical properties $\epsilon_r = 55.0$ and $\sigma = 1.45$ S/m and is imbedded in normal brain tissue with $\epsilon_{r_{ext}} = 42.047$ and $\sigma_{ext} = 0.877$ S/m at 915 MHz. It

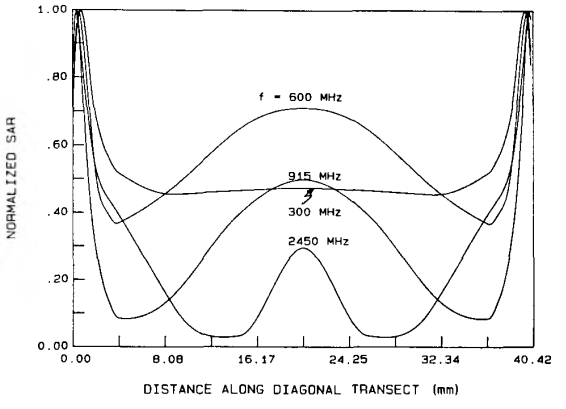


Fig. 12. Normalized SAR for interstitial antenna array shown in Fig. 2 as a function of frequency. $\epsilon_{r_{ext}} = 42.047$, $\sigma_{ext} = 0.877$ S/m.

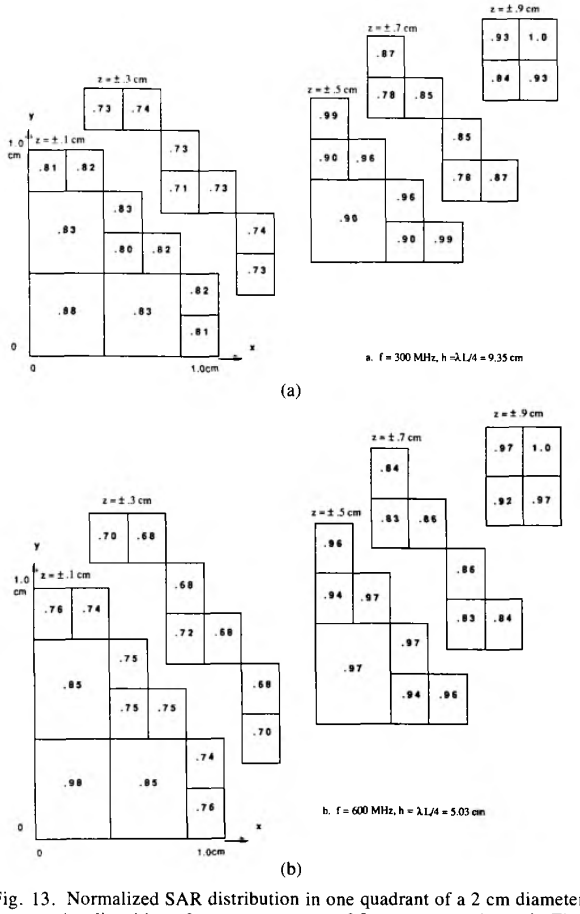


Fig. 13. Normalized SAR distribution in one quadrant of a 2 cm diameter tumor irradiated by a 3 cm square array of four antennas shown in Fig. 2. $\epsilon_{r_{ext}} = 42.047$, $\sigma_{ext} = 0.877$ S/m, $\epsilon_{r_{tumor}} = 55.0$, $\sigma_{external} = 1.45$ S/m. (a) $f = 300$ MHz, $h = k_L/4 = 9.35$ cm. (b) $f = 600$ MHz, $h = k_L/4 = 5.03$ cm.

is irradiated by the 3 cm square array shown in Fig. 2 and described above. The resulting normalized SAR distribution is shown in Fig. 11. This smaller tumor has normalized SAR as much as 20 percent higher in its core than in its periphery. This represents proportionally less excess core heating than in the larger tumor.

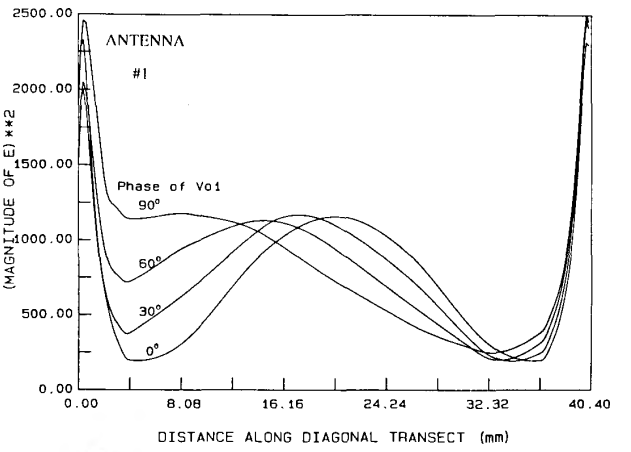


Fig. 14. $|\bar{E}|^2$ V$^2$/m$^2$) for interstitial antenna array shown in Fig. 2 as a function of phase of antenna no. 1. $V_{01} = 1.0\underline{/\theta}$, $V_{02} = V_{03} = V_{03} = V_{04} = 1.0\underline{/\theta}$.

Part of the reason for the inadequate peripheral heating of large tumors by the array shown in Fig. 2 is that, besides high fields around each antenna, the incident field is maximum at the tumor center due to constructive interference between the fields of the array elements and decreases rapidly toward its edges as can be seen in Fig. 3. Reducing the driving frequency of the antennas provides a more uniform incident field within the tumor as shown in Fig. 12.

The effect of reducing the driving frequency on the uniformity of the power deposition in large tumors is examined using the same 2 cm-diameter (approximately) spherical tumor originally shown in Fig. 10. This tumor has $\epsilon_r = 55.0$ and $\sigma = 1.45$ S/m, is imbedded in host tissue having $\epsilon_{r_{ext}} = 42.047$ and $\sigma_{ext} = 0.877$ S/m, and is irradiated by the 3 cm square array shown in Fig. 2. Normalized SAR distributions for frequencies $f = 300$, 600, and 915 MHz are shown in Figs. 13(a), (b), and 10, respectively. The power deposition pattern is most uniform for $f = 300$ MHz which has at most 20 percent higher SAR in the core than periphery, compared with 30 percent for 600 MHz and 55 percent for 915 MHz.

Although decreasing the driving frequency does provide a more uniform power deposition in the tumor, it has the significant drawback of requiring longer antennas which may be physically unfeasible. At 300 MHz, for instance, a quarter-wave antenna has a half-length $h = \lambda_L/4 = 9.35$ cm, compared with 3.47 cm for 915 MHz. The following section examines an alternative approach for achieving uniform heating of large tumors.

## V. Controlling the Power Deposition Pattern using Phase and Amplitude Steering in an Interstitial Antenna Array

A possible method to provide more uniform temperature distribution within large tumors without decreasing driving frequency and hence increasing the antenna length is to steer the electromagnetic energy around the periphery of the tumor, heating several smaller sections of the tumor in sequence. Two methods of steering electromag-

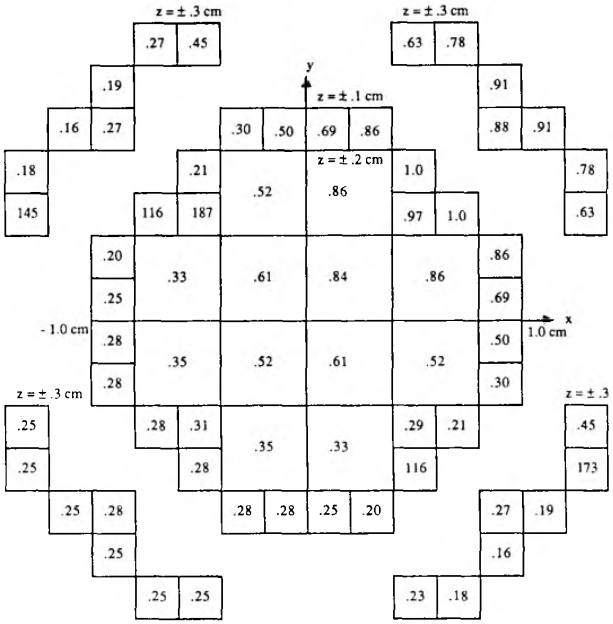


Fig. 15. SAR (W/kg) distribution in 2 cm diameter tumor irradiated by the 3 cm square array of four antennas shown in Fig. 2. $\epsilon_{r_{ext}} = 42.047$, $\sigma_{ext} = 0.877$, $\epsilon_{r_{tumor}} = 55.0$, $\sigma_{tumor} = 1.45$ S/m. $V_{01} = 0.1\angle 90°$, $V_{02} = V_{03} = V_{04} = 1.0\angle 0$.

netic energy within interstitial antenna arrays were examined—varying the relative phases of the antenna-driving-point voltages, and varying the relative magnitudes of the feed voltages. The effect of varying the phases of two antennas in a 2 cm square array has been studied by Trembly [16].

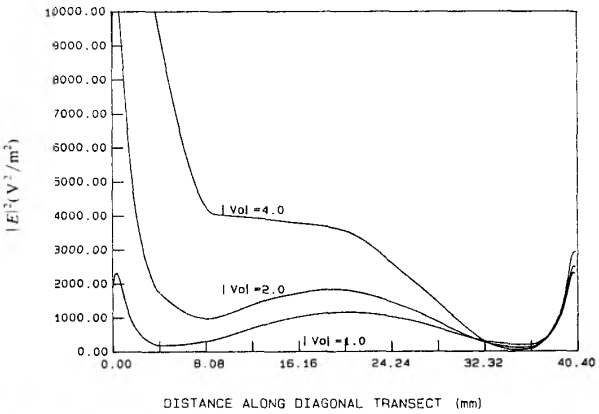


Fig. 16. $|\bar{E}|^2$ ($V^2/m^2$) for interstitial antenna array shown in Fig. 2 as a function of magnitude of driving voltage on antenna no. 1.

The effect of changing the phase of one antenna in the array (Fig. 2) on the incident fields is shown in Fig. 14. The electromagnetic energy shifts toward the phase lead, and a +90° phase change shifts the energy about 1 cm toward the leading antenna. This shift is sufficient to allow sequential heating of a 2 cm-diameter tumor. The result of this +90° phase change on the large tumor previously examined in Fig. 10 can be seen in Fig. 15. Steering with +90° on one antenna causes the power deposition in the external cells to be as much as 50 percent higher than in the core cells, as compared to periphery as much as 55 percent lower than core for no steering.

The possibility of further steering the power deposition by altering the magnitude of the driving point voltage was also examined. The effect of changing the voltage magnitude on the no. 1 antenna in the array (Fig. 2) is shown in Fig. 16 for two cases where voltages in antenna no. 1 were two and four times the values on the remaining elements of the array. Fig. 16 shows that amplitude modulation is capable of noticeably steering the power deposition pattern. Because of the required large changes in the magnitudes of the applied voltages and the need to use attenuators for this purpose, the process of achieving pattern steering using magnitude variation is less desirable.

## VI. Conclusion

In this paper we have presented a three-dimensional numerical model for analyzing the electromagnetic power deposition pattern in a tumor of arbitrary shape and electrical properties being heated by an interstitial array of insulated antennas. It was assumed that coupling between the antennas could be neglected and that the antennas were sufficiently insulated so that the scattered field from the tumor would not affect their radiation patterns.

Results were presented to show the need to include the effects of the geometry and electrical properties of the tumor in modeling its absorbed EM power. Excess tumor core heating was examined as a function of frequency and tumor size. Methods to control the power deposition pattern by varying the phase or driving point voltage of one antenna in the array were also examined and their use for

sequentially heating small portions of large tumors was discussed.

Future modeling efforts should include the effects of coupling the antennas to allow array spacing to be decreased and to include the impact of the scattered field from the tumor on the radiation pattern of the array. The numerical model could also be improved by using more complex basis functions than the pulse basis expansion function to provide quantitatively more accurate results with improved computational efficiency. Research efforts are underway to implement some of these aspects in our future calculations.

## Appendix A
## Fields of an Insulated Antenna

A simple insulated antenna is shown in Fig. 17. It is made up of an inner conductor (assumed perfectly conducting) of radius $a$ and half-length $h$ surrounded by insulating dielectric of radius $b$ and permittivity $\epsilon_{r_2}$. This is imbedded in a conducting dielectric medium with electrical properties $\epsilon_{r_{ext}}$ and $\sigma_{ext}$. The fields outside the antenna given by [10] as

$$E_{4z}(\rho, z) = \frac{j\omega\mu_0 I_0}{4\pi \sin k_L h}\left\{\left(1 - \frac{k_L^2}{k_4^2}\right)\cdot\int_{-h}^{h}\sin k_L(h - z')\left[\psi(z, z') + \psi(z, -z')\right]dz' + \frac{k_L}{k_4^2}\left[\psi z, h\right) + \Psi(z, -h) - 2\psi(z, 0)\cos k_L h\right]\right\}$$

$$E_{4\rho}(\rho, z) = -\frac{j\omega\mu_0 I_0}{4\pi \sin k_L h}\left\{\frac{k_L\rho}{k_4^2}\cdot\int_{-h}^{h}\cos k_L(h - z')\cdot\left[\left(\frac{jk_4}{R_1} - \frac{1}{R_1^2}\right)\psi(z, z') \right. \quad \text{(A1)}$$

$$\left. - \left(\frac{jk_4}{R_2} - \frac{1}{R_2^2}\right)\psi(z, z')\right]\right\}. \quad \text{(A.2)}$$

Constants used in (A.1), (A.2), and (A.3) are given by

$$k_2 = \omega(\mu_0\epsilon_0\epsilon_{r_2})^{1/2}$$

$$k_4 = k_{ext} = \omega(\mu_0\epsilon_{ext}^*)^{1/2}$$

$$R_1 = \left[(z - z')^2 + \rho^2\right]^{1/2}$$

$$R_2 = \left[(z + z')^2 + \rho^2\right]^{1/2}$$

$$\psi(z, z') = \frac{e^{jk_4R_1}}{R_1}, \qquad \psi(z, -z') = \frac{e^{jk_4R_2}}{R_2}.$$

The driving point current is

$$I_0 = V_0/Z_0. \quad \text{(A.3)}$$

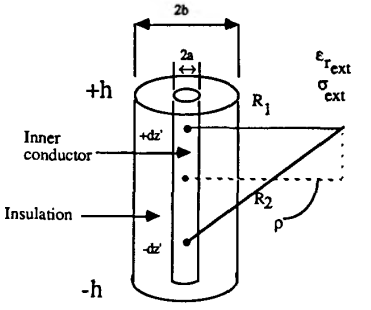

Fig. 17. Insulated antenna.

For $e^{j\omega t}$ time dependence, the input impedance $Z_0$ is given for a dipole antenna by

$$Z_0 = 2jZ_c \cot k_L h \quad \text{(A.4)}$$

where

$$Z_c = \left(\frac{\omega\mu_0 k_L}{2\pi k_2^2}\right)\left[\ln(b/a) + n_{24}^2 F\right]. \quad \text{(A.5)}$$

$$k_L = k_2\frac{\left[\ln(b/a) + F\right]^{1/2}}{\left[\ln(b/a) + n_{24}^2 F\right]^{1/2}} \quad \text{(A.6)}$$

$$n_{24}^2 = k_2^2/k_4^2$$

$$F = \frac{H_0^{(1)}(k_4 b)}{k_4 b H_1^{(1)}(k_4 b)}.$$

This analysis is subject to the constraints

$$\left|k_4/k_2\right|^2 \gg 1; \quad (k_2 b)^2 \ll 1 \quad \text{and} \quad R_1^2 \gg b^2, \quad R_2^2 \gg b^2.$$

The integrals in (A.1) and (A.2) are obtained numerically using Gauss-quadrature integration with 48 points. It should be noted that the fields at or very near the surface of the insulation were obtained using spline interpolation procedure similar to that described in [7]. In this procedure the very near fields $\rho \leq 2b$ in the ambient medium were fit by a spline to the fields inside the insulation through the application of the boundary conditions.

## References

[1] G. Samaras, "Intracranial microwave hyperthermia: Heat induction and temperature control," *IEEE Trans. Biomed. Eng.*, vol. BME-31, pp. 63-69, Jan. 1984.

[2] L. S. Taylor, "Implantable radiators for cancer therapy by microwave hyperthermia," *Proc. IEEE*, vol. 68, pp. 142-149, Jan. 1980.

[3] A. Winter, J. Laing, R. Paglione, and F. Strezer, "Microwave hyperthermia for brain tumors," *Neurosurg.*, vol. 17, pp. 387-399, 1985.

[4] H. T. Law and R. T. Pettigrew, "New apparatus for the induction of localized hyperthermia for the treatment of neoplasia," *IEEE Trans. Biomed. Eng.*, vol. BME-26, pp. 175-177, Mar. 1979.

[5] J. G. Short and P. F. Turner, "Physical hyperthermia and cancer therapy," *Proc. IEEE*, vol. 68, pp. 133-142, Jan. 1980.

[6] E. G. Cravahlo, L. Fox, and J. C. Kan, "The application of the bioheat equation to the design of thermal protocols for local hyperthermia," *Annals of New York Acad. Sci.*, vol. 335, pp. 86-97, Mar. 31, 1980.

[7] B. S. Trembly, "The effects of driving frequency and antenna length on power deposition within a microwave antenna array used for hyperthermia," *IEEE Trans. Biomed. Eng.*, vol. BME-32, pp. 152-157, Feb. 1985.

[8] R. Peloso, D. T. Tuma, and R. K. Jain, "Dielectric properties of solid tumors during normothermia and hyperthermia," *IEEE Trans. Biomed. Eng.*, vol. BME-31, pp. 725-728, Nov. 1984.

[9] K. R. Foster and J. L. Schepps, "Dielectric properties of tumor and normal tissues at radio through microwave frequencies," *J. Microwave Power*, vol. 16, pp. 107-119, 1981.
[10] J. L. Schepps and K. R. Foster, "The UHF and microwave dielectric properties of normal and tumour tissues: Variation in dielectric properties with tissue water content," *Phys. Med. Biol.*, vol. 25, pp. 1149-1159.
[11] G. M. Hahn, P. Kernahan, and A. Martinez, "Some heat transfer problems associated with heating by ultrasound, microwaves, or radio frequency," *Annals New York Acad. Sci.*, vol. 335, pp. 327-346, Mar. 31, 1980.
[12] A. W. Guy and C.-K. Chou, "Physical aspects at localized heating by radiowaves and microwaves," in *Hyperthermia in Cancer Therapy*, F. K. Storm, Ed. Boston, MA: G. K. Hall Med., 1983, pp. 279-304.
[13] D. Livesay and K.-M. Chen, "Electromagnetic fields induced inside arbitrarily shaped biological bodies," *IEEE Trans. Microwave Theory Tech.*, vol. MTT-22, pp. 1273-1280, Dec. 1974.
[14] J. Van Bladel, "Some remarks on Green's dyadic for infinite space," *IRE Trans. Antennas Prop.*, vol. AP-9, pp. 563-566, Nov. 1961.
[15] R. W. P. King, B. S. Trembly, and J. W. Strohbehn, "The electromagnetic field of an insulated antenna in a conducting or dielectric medium," *IEEE Trans. Microwave Theory Tech.*, vol. MTT-31, pp. 574-583, July 1983.
[16] B. S. Trembly, H. Wilson, M. J. Sullivan, A. D. Stein, T. Z. Wong, and J. W. Strohbehn, "Control of the SAR pattern within an interstitial microwave array through variation of antenna driving phase," *IEEE Trans. Microwave Theory Tech.*, vol. MTT-34, pp. 568-571, May 1986.
[17] H. Massoudi, C. H. Durney, and M. F. Iskander, "Limitations of the cubical block model of man in calculating SAR distributions," *IEEE Trans. Microwave Theory Tech.*, vol. MTT-32, pp. 746-751, Aug. 1984.

**Cynthia M. Furse** was born in Stillwater, ME, in 1963. She received the B.S.E.E. degree with a mathematics minor and the M.S.E.E. degree from the University of Utah, Salt Lake City, in 1986 and 1988, respectively.

She has been a research assistant at the University of Utah since 1986, and was a summer research engineer with Chevron Oil Field Research Company in 1986. She is currently pursuing the Ph.D. degree in electrical engineering at the University of Utah. Her research interests are in the area of numerical modeling of wave propagation and scattering in complex media.

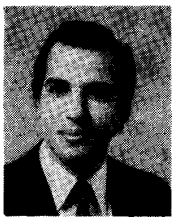

**Magdy F. Iskander** (S'72-M'76-SM'84) was born in Alexandria, Egypt, on August 6, 1946. He received the B.Sc degree in electrical engineering from the University of Alexandria, Egypt, in 1969. He received the M.Sc. and Ph.D. degrees in 1972 and 1976, respectively, in microwaves, from the University of Manitoba, Winnipeg, Manitoba, Canada.

In 1976, he was awarded a National Research Council of Canada Postdoctoral Fellowship at the University of Manitoba. Since 1977 he has been with the Department of Electrical Engineering and the Department of Bioengineering at the University of Utah, Salt Lake City, where he is currently a Professor of Electrical Engineering and a Research Professor of Materials Science and Engineering. In 1981, he received the University of Utah President David P. Gardner Faculty Fellow Award and spent the academic quarter on leave as a Visiting Associate Professor at the Department of Electrical Engineering and Computer Science, Polytechnic Institute of New York, Brooklyn. He spent the 1985 and 1986 summers at Chevron Oil Field Research Company, La Habra, CA, as a Visiting Scientist. From September 1986 to May 1987 he spent a sabbatical leave at UCLA where he worked on the coupling characteristics of microwave integrated circuits to inhomogeneous media, and at the Harvey Mudd College where he learned about their engineering clinic program. He spent the last four months of the sabbatical leave with Ecole Superieure d'Electricite, Gif-Sur-Yvette, France, where he worked on microwave imaging. His present fields of interest include the use of numerical techniques in electromagnetics to calculate scattering by dielectric objects, antenna design for medical applications, microwave integrated circuit design, and the use of microwave methods for materials characterization and processing. He edited two special issues of the *Journal of Microwave Power*, one on "Electromagnetics and Energy Applications," March 1983, and the other on "Electromagnetic Techniques in Medical Diagnosis and Imaging," September 1983. He has seven patents, contributed seven chapters to five research books, published more than 80 papers in technical journals, and made more than 150 presentations at technical conferences.

Dr. Iskander received the College of Engineering Outstanding Teaching Award and the College Patent Award for creative, innovative, and practical invention in 1983. In 1984, he was selected by the Utah Section of IEEE as the Engineer of the Year. In 1984, he received the Outstanding Paper Award from the International Microwave Power Institute. In 1985, he received the Curtis W. McGraw ASEE National Research Award for outstanding early achievements by a University Faculty member. He established the Engineering Clinic Program in the College of Engineering at the University of Utah. Since then the program has attracted 17 research projects from nine different companies throughout the United States. He is also a member of the IEEE AP-S National Committee on Education and Chairman of the Subcommittee on the use of computational techniques in electromagnetic education.